OXFORD

Cerebral Cortex, 2023, **33**, 135–151
https://doi.org/10.1093/cercor/bhac057
Advance access publication date 7 April 2022
Original Article

Altered linear coupling between stimulus-evoked blood flow and oxygen metabolism in the aging human brain

Monroe P. Turner[1,2], Yuguang Zhao[1,2], Dema Abdelkarim[1,2], Peiying Liu[3], Jeffrey S. Spence[1,2], Joanna L. Hutchison[1,2], Dinesh K. Sivakolundu[1,4], Binu P. Thomas[5], Nicholas A. Hubbard[6], Cuimei Xu[3], Kamil Taneja[3], Hanzhang Lu[3], Bart Rypma[1,2,*]

[1]School of Behavioral and Brain Sciences, University of Texas at Dallas, Richardson, TX 75080, USA,
[2]Center for BrainHealth, University of Texas at Dallas, Dallas, TX, 75235, USA,
[3]Department of Radiology and Radiological Science, Johns Hopkins University, Baltimore, MD 21287, USA,
[4]Department of Biological Sciences, University of Texas at Dallas, Richardson, TX, 75080, USA,
[5]Advanced Imaging Research Center, University of Texas Southwestern Medical Center, Dallas, TX 75235, USA,
[6]Department of Psychology, Center for Brain, Biology, and Behavior, University of Nebraska, Lincoln, NE 68588, USA

*Corresponding author: School of Behavioral and Brain Sciences, Center for Brain Health, University of Texas at Dallas, 800 West Campbell Road, Richardson, TX 75080, USA. Email: bart.rypma@utdallas.edu

Neural-vascular coupling (NVC) is the process by which oxygen and nutrients are delivered to metabolically active neurons by blood vessels. Murine models of NVC disruption have revealed its critical role in healthy neural function. We hypothesized that, in humans, aging exerts detrimental effects upon the integrity of the neural-glial-vascular system that underlies NVC. To test this hypothesis, calibrated functional magnetic resonance imaging (cfMRI) was used to characterize age-related changes in cerebral blood flow (CBF) and oxygen metabolism during visual cortex stimulation. Thirty-three younger and 27 older participants underwent cfMRI scanning during both an attention-controlled visual stimulation task and a hypercapnia paradigm used to calibrate the blood-oxygen-level-dependent signal. Measurement of stimulus-evoked blood flow and oxygen metabolism permitted calculation of the NVC ratio to assess the integrity of neural-vascular communication. Consistent with our hypothesis, we observed monotonic NVC ratio increases with increasing visual stimulation frequency in younger adults but not in older adults. Age-related changes in stimulus-evoked cerebrovascular and neurometabolic signal could not fully explain this disruption; increases in stimulus-evoked neurometabolic activity elicited corresponding increases in stimulus-evoked CBF in younger but not in older adults. These results implicate age-related, demand-dependent failures of the neural-glial-vascular structures that comprise the NVC system.

Key words: neurovascular coupling; aging; calibrated fMRI; cerebral blood flow; cerebral oxygen metabolism.

Introduction

Neural activity within a given region of the brain is constantly shifting in response to exogenous stimuli (Ogawa et al. 1992), cognitive processes (Le Bihan et al. 1993), and intra- and internetwork connection signaling (Biswal et al. 1995). Lacking local reserves of energy (e.g. glycogen storage), neurons depend upon astrocytes to relay their activity-related metabolic needs by signaling blood vessels to dilate in response to increases in neurometabolic activity (Attwell et al. 2010). Research using murine models has elucidated fundamental molecular and cellular mechanisms that comprise this neural-vascular coupling (NVC) process. At excitatory synapses, astrocytic endfeet uptake glutamate (Gottfried et al. 2002) and potassium ions (Jukkola et al. 2013) following action potentials. Astrocytes then signal local vasculature to dilate through deposition of epoxyeicosatrienoic acid and prostaglandins, thus increasing local blood flow and oxygen (O_2) delivery (i.e. functional hyperemia; Jukkola et al. 2013). Dual-echo calibrated functional magnetic resonance imaging (cfMRI Hyder, 2004; Hoge, 2012) permits specific measurement of each component of a three-tier neural-glial-vascular model. Neurometabolic activity can be functionally indexed by the rate of oxygen metabolism by neurons (tier I), calculated using a scaled product of measured blood flow and blood-oxygen-level-dependent (BOLD) signal. The function of neural-vascular mediators, such as astrocytes (Metea and Newman 2006; Takano et al. 2006; Attwell et al. 2010; Tian et al. 2010; Petzold and Murthy 2011; Lee et al. 2012; MacVicar and Newman 2015; Cauli and Hamel 2018; Gu et al. 2018) as well as others such as endothelial cells (Chen et al. 2014; Hillman 2014) and pericytes (Krueger and Bechmann 2010; Dalkara et al. 2011), can be indexed by the proportion of blood flow increase per unit change in neural oxygen metabolism (tier II). Vascular activity (cerebral arterioles and capillaries, tier III) can be functionally indexed by direct measurement of blood flow.

Healthy aging affects NVC (for review, see Abdelkarim et al. 2019; Tsvetanov et al. 2021). However, precisely which constituent processes of NVC are altered in healthy aging remains unknown. We hypothesize that, as neurometabolic demand increases, adverse effects on neural function aggregate due to the inability of metabolite supply to keep pace with metabolic demand (the

Received: July 22, 2021. **Revised:** January 13, 2022. **Accepted:** January 14, 2022

metabolic insufficiency hypothesis; Shetty et al. 2011; Turner 2021; see also Zhao et al. 2021). Mitochondrial production of adenosine triphosphate (ATP) decreases with age (Harper et al. 2004), while concentrations of reactive oxygen species increase (Leutner et al. 2001), damaging cells and disrupting calcium homeostasis (Chandran et al. 2019). This age-related oxidative stress also disrupts functional hyperemia by limiting nitric oxide signaling and damaging vascular endothelial cells (Podlutsky et al. 2009; Trott et al. 2011), leading to stiffening of arteries and arterioles (Kohn et al. 2015; Zimmerman et al. 2021). Oxidative stress may also limit the ability of astrocytes to produce functional hyperemia in healthy aging (cf. Jiang and Cadenas 2014; Abdelkarim et al. 2019). In this case, age-related impairment of NVC would also be expected to disrupt coordination of the fundamental supply–demand relationship between neurometabolic activity and subsequent delivery of nutrients to neurons. Previous work by Hutchison, Lu, et al. (2013) and Hutchison, Shokri-Kojori, et al. (2013) used cfMRI to explore age-reductions in BOLD signal in terms of the underlying neurophysiologic quantities of relative cerebral metabolic rate of oxygen ($CMRO_2$, tier I), the NVC ratio (tier II), and relative cerebral blood flow (CBF, tier III) in response to visual stimulation. Their observation of age-equivalent blood flow despite age-related increases in oxygen metabolism, yielding a significantly greater NVC ratio in younger than in older adults, supports the hypothesis of age-related disruption of the glial intermediaries of the neural-glial-vascular system.

Effects of metabolic demand on neural systems complicate interpretations of results from studies of healthy human aging which invoke assumptions related to the NVC system. NVC is affected by different aspects of experimental paradigms in functional magnetic resonance imaging (fMRI) research, including the nature of a presented stimulus (e.g. duration, intensity; Liang et al. 2013), the parameters of the task that participants perform (e.g. task difficulty, speed/accuracy demands; Moradi et al. 2012), or alteration of vascular tone from exogenous neuropharmacological agents (e.g. caffeine; Perthen et al. 2008; Griffeth et al. 2011). The strength of NVC also varies spatially as a function of cortical region (Chiarelli et al. 2007; Ances et al. 2009). In the present study, building on prior work (Hutchison, Lu, et al. 2013; Hutchison, Shokri-Kojori, et al. 2013), we modulated demand on the NVC system in occipital lobe by parametrically varying the frequency of a visual stimulus presented to older and younger participants during measurement of BOLD and its neurophysiologic constituents using calibrated fMRI scanning.

Materials and methods

Participants

A total of 60 participants were enrolled in this study at 2 sites. Thirty-three younger ($M_{age} = 22.5$, $SD_{age} = 3.3$, 14 female) and 27 older ($M_{age} = 60.5$, $SD_{age} = 6.8$, 17 female) participants were recruited from the greater Dallas-Fort Worth Metroplex and the Baltimore-Washington metropolitan area through posted flyers, advertisements placed online and through local radio stations, and word-of-mouth referrals. All participants provided informed written consent prior to scanning, and all were compensated financially for their participation. Procedures were jointly approved by the Institutional Review Boards of the University of Texas at Dallas, the University of Texas Southwestern Medical Center, and Johns Hopkins University.

Participants were screened for eligibility prior to study enrollment. General exclusion criteria were the presence of any intracranial or intraocular metal, or implanted devices (e.g. pacemaker, neurostimulation system), or if they were pregnant or claustrophobic. To limit additional risk or discomfort during hypercapnia, exclusion criteria also included a history of chronic obstructive pulmonary disease, interstitial lung disease, asthma, sarcoidosis, tuberculosis, asbestosis, silicosis, emphysema, systemic lupus erythematosus, pulmonary hypertension, or airway obstruction. To control for potential vascular confounds, exclusion criteria also included a history of transient ischemic attack, cerebrovascular accident (stroke), arteriovenous malformation, cardiac disease, angina, myocardial infarction (heart attack), congestive heart failure, coronary artery bypass graft, heart arrhythmia, migraine headaches (depending on frequency and the incidence of aura), or smoking (defined as smoking >1 cigarette a day, >3 times a week).

Experimental paradigm

Protocol

Inclusion and exclusion criteria were confirmed on the day of scanning. To account for potential effects on perfusion measurements due to caffeine or nicotine ingestion (Tsvetanov et al. 2021), each participant completed a questionnaire that ascertained their last consumption of caffeine, alcohol, nicotine, and any prescription or nonprescription drugs as well as any exercise and/or health supplements within 24 h prior to scanning. Once the participant entered the scanner room, a mouthpiece and a nose clip were positioned for the breathing challenge (see "Hypercapnia task"). The participant was then scanned for approximately 12 min (comprising the dual-echo cfMRI scan as well as phase-contrast (PC) under both normocapnic and hypercapnic conditions) and was withdrawn from the scanner bore afterwards. The hypercapnia apparatus was then removed, and the participant once again entered the scanner and completed 3 runs of a visual task (see "Visual task"), lasting approximately 20 min. For the remainder of the time the participant spent in the scanner, structural scans were collected (approximately 25 min; see "Structural MRI scanning parameters"). Total scan time was approximately 1 h.

Hypercapnia task

To permit calculation of $CMRO_2$, a hypercapnic breathing challenge was employed in which the participant breathed both room air and an iso-oxic CO_2 solution (medical-grade gas composed of 74% N_2, 21% O_2, and

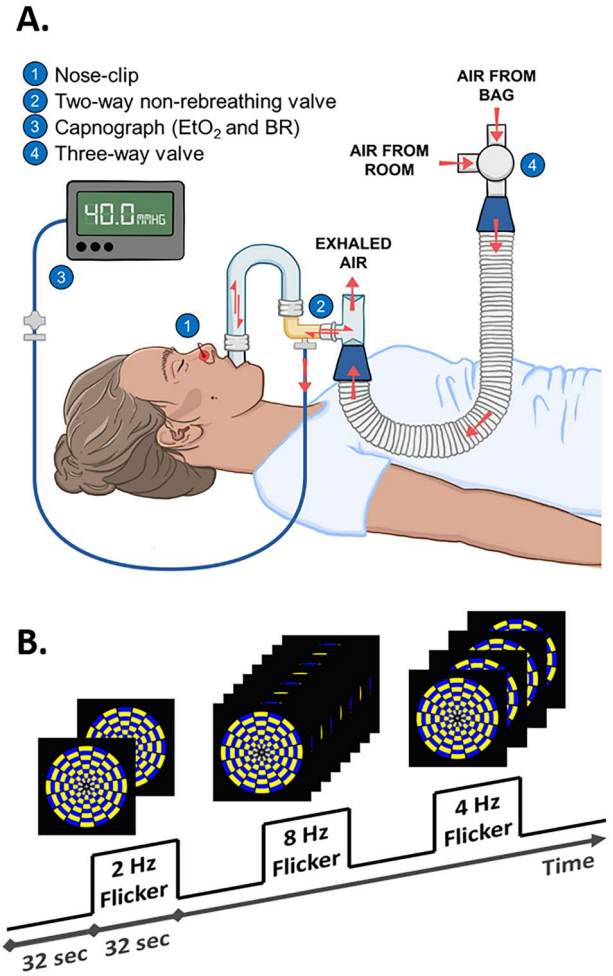

Fig. 1. Depictions of (A) the hypercapnia apparatus and of (B) the paradigm and flickering checkerboard stimulus used in the visual task.

5% CO_2). A mouthpiece and nose clip were positioned to ensure breathing could only occur by mouth (see Fig. 1A). During this part of scanning, the participant breathed room air through the mouthpiece for approximately 4 min, followed by the CO_2 solution for approximately 6 min. A researcher inside the scanner room (at sufficient distance to not affect field homogeneity) monitored the participant's vital signs and switched the breathing valve between room-air and CO_2 once 4 min had passed. After scanning, the researcher switched the breathing valve back to room air, and the participant was removed from the scanner.

Visual task

The visual task was block-designed to maximize signal detection power (Birn et al. 2002) and to accommodate the effective repetition time (TR) of the dual-echo sequence (see "cfMRI scanning parameters"). The task was presented in 3 sequential runs, each containing 6 task blocks and 6 rest blocks. Task blocks were alternated with rest blocks, each 32 s long (both task blocks and rest blocks), and each run began with a rest block and ended with a task block (see Fig. 1B).

During rest blocks, a single fixation cross was presented on a black background. During task blocks, a single fixation cross was presented at the center of a radial yellow and blue flickering checkerboard that maximized contrast. The frequency of the flicker was parametrically modulated between 2, 4, and 8 Hz (Cliff et al. 2013) to vary the frequency of visual cortex stimulation. Flicker frequency presentation was pseudorandomized with the constraints that each condition did not follow linear, quadratic, or cubic patterns, and every condition occurred an equal number of times (i.e. twice) per run. To ensure the consistency of the participant's focus of attention, the fixation cross presented at center screen changed in luminance every 2–6 s (mean = 4 s) throughout the task (through both task and rest blocks). Participants were instructed to indicate via thumb button press each time they saw the luminance of the cross change. Each run lasted 6 min and 24 s (48 dynamics), and all 3 runs lasted 19 min and 12 s.

MRI data acquisition

Imaging data were collected at 2 sites: (i) the Advanced Imaging Research Center at the University of Texas Southwestern Medical Center and (ii) the Department of Radiology at the Johns Hopkins University School of Medicine. Data at both sites were collected on identical-model Philips Achieva 3 Tesla magnetic resonance imaging (MRI) scanners (Philips Medical Systems, Best, the Netherlands). Both scanners were equipped with 32-channel SENSE head coils. Prior to data collection, an equivalence study was performed using the same participant (1 of the authors, H.L.) to ensure that signal measured in both scanning environments did not show site effects.

Structural MRI scanning parameters

A T1-weighted magnetization-prepared rapid gradient-echo (MPRAGE) was used to acquire structural MRI data in 160 sagittal slices (no gap), each containing a 256×256 matrix of 1 mm^3 isovoxels (flip angle = 12°, echo time = 3.7 ms, TR = 8.1 ms).

cfMRI scanning parameters

A pseudo-continuous arterial spin labeling (pCASL) sequence (Alsop et al. 2015; Aslan et al. 2010) without background or vascular suppression was used to acquire dual-echo fMRI data with echo times at $TE_1 = 13$ ms and $TE_2 = 30$ ms, and TR = 4,000 ms (flip angle = 90°, multislice echo-planar-imaging acquisition, 22 transverse slices parallel to the AC-PC plane, voxel size $3.44 \times 3.44 \times 6$ mm^3, labeling duration = 1,400 ms, postlabeling delay = 1,450 ms). Data from Echo 1 were used to obtain CBF-weighted images, and data from Echo 2 were used to obtain BOLD images. Acquisition geometry for functional volumes was situated to ensure whole-brain coverage, with emphasis placed on acquiring both occipital (visual) and precentral (motor) cortices.

During the hypercapnia session, in order to account for variations in pCASL labeling efficiency during CO_2 inhalation (Aslan et al. 2010), PC quantitative flow MRI scans were performed before and after the cfMRI sequence. Global flow values were used to correct for individual differences in pCASL labeling efficiency using procedures described previously (Hutchison, Lu, et al. 2013; Hutchison, Shokri-Kojori, et al. 2013).

Structural MRI data processing

Freesurfer was used for cortical parcellation and reconstruction of T1-weighted images using the "recon-all" function (Fischl 2012). Individual regions of interest (ROIs) were generated in participants' native space by segmentation of the reconstructed T1-weighted images using labels from the Desikan-Killiany atlas (Desikan et al. 2006). The structural ROI we selected to represent occipital (visual) cortex comprised cuneus, lingual gyrus, lateral occipital gyrus, and pericalcarine cortex (that surrounding the calcarine fissure) and was generated using Freesurfer's "mri_label2vol" function.

cfMRI data preprocessing

Figure 2 depicts a diagram of the preprocessing workflow for cfMRI data. Raw images were converted to AFNI's HEAD/BRIK format, as AFNI was used for all preprocessing and first-level data analysis. Images were checked for spikes using AFNI's "3dDespike" function (values >4 standard deviations (SDs) above the mean value), and any detected spikes were attenuated to between 2.5 and 4 SDs above the mean value based on their location in the distribution of values in the volume. BOLD images (i.e. Echo 2 images) from each run were motion-corrected using AFNI's "3dvolreg" function by a 6-degree-of-freedom rigid-body transformation (3 translation and 3 rotation parameters) to the fifth functional volume within the time-series of the run. Due to the inherently greater gray-white contrast of BOLD data relative to pCASL (i.e. Echo 1) data, and because data from both echoes were gathered with identical geometry, the transformation matrix output by AFNI's "3dvolreg" function for BOLD volumes was applied to pCASL volumes. Volumes from subsequent runs of the task were coregistered to volumes from the first run of the task using AFNI's "3dAllineate" function.

Relative CBF maps were generated from pCASL label and control images using the surround-subtraction method (Liu and Wong 2005; Lu et al. 2006). Surround-subtraction minimizes BOLD influence on relative CBF data and upsamples those data (Echo 1) to an effective TR of 4 s, matching the TR of the BOLD (Echo 2) data. BOLD volumes were averaged with neighboring BOLD volumes in time to remove the contaminating effects of the pCASL labeling pulse prior to acquisition of label images to attenuate high-frequency noise in the BOLD time-series data (Liu and Wong 2005; Hutchison, Lu, et al. 2013; Hutchison, Shokri-Kojori, et al. 2013; Hubbard et al. 2017; Sivakolundu et al. 2020; West et al. 2021). Functional data were then coregistered to a participant's structural T1 image in native space using AFNI's "align_epi_anat.py" script, which exhibited superior intermodal coregistration performance compared to AFNI's "3dAllineate" function and resampled into structural-resolution voxels (1 mm^3). Data were then spatially smoothed by convolving an 8-mm FWHM Gaussian kernel with BOLD and relative CBF volumes, high-pass filtered to remove low-frequency artifacts (e.g. scanner drift), and extracranial voxels were removed.

cfMRI data analysis

To calculate percent signal change (PSC) estimates for each modality (BOLD and CBF; Davis et al. 1998; Hoge et al. 1999a, 1999b), a reduced general linear model (GLM) was run with a single boxcar regressor using AFNI's "3dDeconvolve" function to identify voxels where the visual task reliably elicited signal. The resulting parameter map was intersected with the occipital ROI generated from Freesurfer, which served as the structural mask. Task data were functionally masked using an approach that allowed an equal number of voxels to be analyzed for each participant and for each condition. *t*-score maps output from the single-regressor GLM were converted to rank-scores within the structural ROI, and a conjunction image was created using the minimum *t*-score of BOLD and relative CBF data (Friston et al. 2005; Hutchison, Lu, et al. 2013; Hutchison, Shokri-Kojori, et al. 2013; see also Schäfer et al. 2012). The top 5,000 voxels of this conjunction image served as the ROI for the initial by-condition analysis, which was then expanded to concentric ROIs of 10,000, 20,000, 30,000, and 40,000 voxels. Three ROIs were chosen for analysis: the focal ROI (the top 5,000 voxels), the proximal ROI (the top 10,000 voxels but not including the focal ROI), and the distal ROI (the top 20,000 voxels but not including the proximal or focal ROIs). Finally, a second GLM used 3 individual boxcar regressors to model PSC in the resulting ROI for each modality (BOLD and relative CBF) and each condition (2, 4, and 8 Hz). The resulting PSC estimates for BOLD and relative CBF from the second GLM were then used in subsequent analyses to calculate both relative $CMRO_2$ and the NVC ratio. It is important to note that these measures all reflect changes from baseline rather than absolute values.

Calculation of M, $CMRO_2$, and NVC ratio

Figure 3 depicts the schematic for the calculation of M, $CMRO_2$, and NVC ratio. The deoxyhemoglobin dilution model of BOLD signal change (Davis et al. 1998; Hoge et al. 1999a, 1999b) allows calculation of $CMRO_2$ change from BOLD signal change and CBF change using the relationship in Equation (1):

$$\frac{\Delta BOLD}{BOLD_0} = M\left(1 - \left(\frac{CMRO_2}{CMRO_{2|0}}\right)^{\beta}\left(\frac{CBF}{CBF_0}\right)^{\alpha-\beta}\right) \quad (1)$$

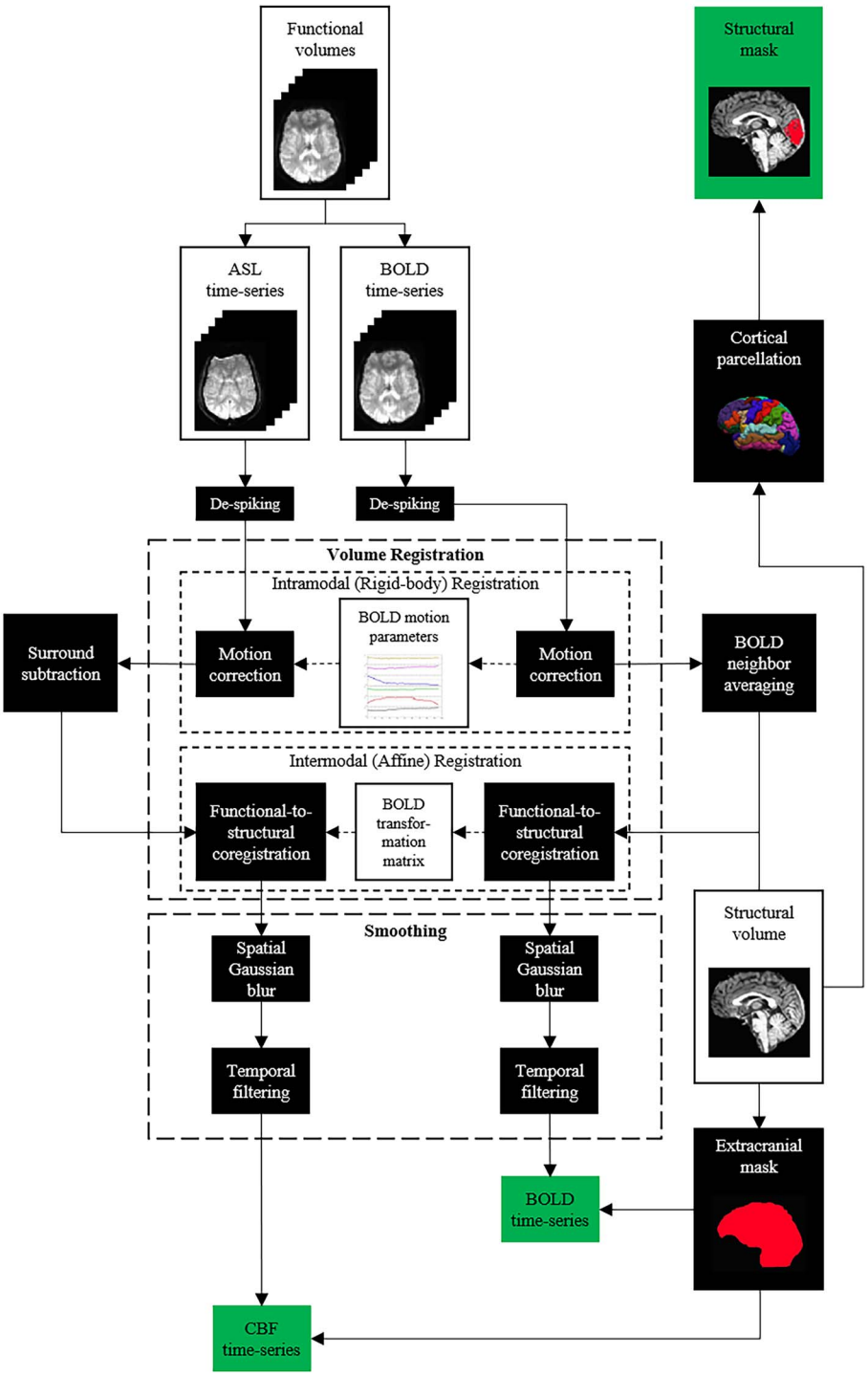

Fig. 2. Preprocessing pipeline for BOLD and relative CBF data.

In Equation (1), M is the calibration constant and can be conceptualized either as a baseline deoxyhemoglobin level (Griffeth and Buxton 2011), or as the theoretical ceiling of BOLD signal change (Bulte et al. 2012), α is a constant relating CBF to cerebral blood volume (Grubb Jr. et al. 1974; Chen and Pike 2009), and β is a constant based on the strength of the magnetic field (Lu and van Zijl 2005). This equation, in addition to the measured quantities of BOLD PSC ($\Delta BOLD/BOLD_0$) and CBF ratio (CBF/CBF_0) and constants α (=0.23) and β (=1.3), contains 2 unknowns. The first of these unknowns and the ultimate goal of the calculation, $CMRO_2$ ratio ($CMRO_2/CMRO_{2|0}$; i.e. $CMRO_2$ PSC/100 + 1), can only be determined after the second unknown, M, has been estimated via the hypercapnia calibration experiment. Because CO_2 is a vasodilator to which cerebral vasculature is particularly sensitive (Ainslie and Burgess, 2008), imaging participants while breathing a 5% CO_2 solution allows for calculation of M relative to BOLD signal change and CBF change under conditions of

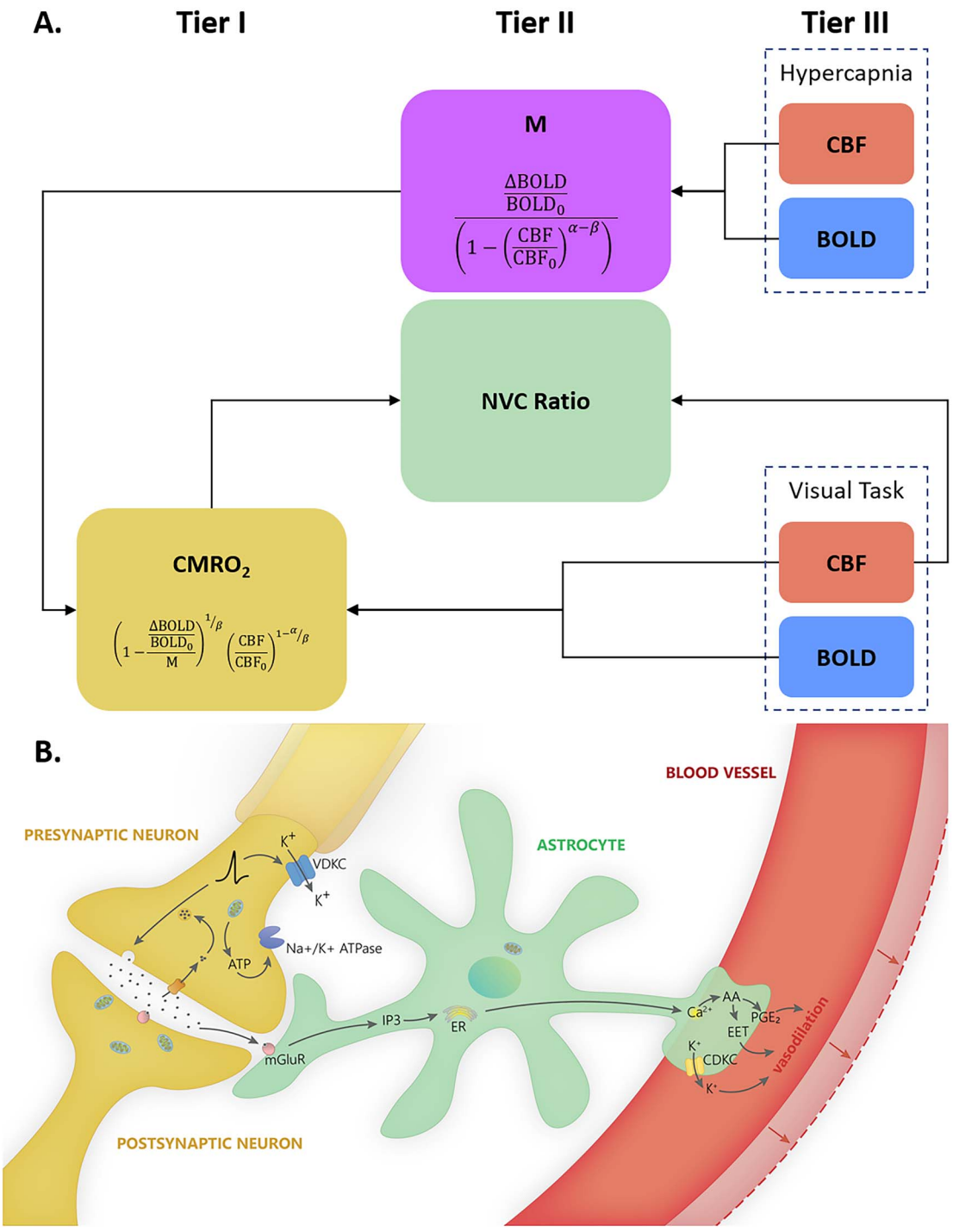

Fig. 3. (A) Schematic for the calculation of M, $CMRO_2$, and NVC ratio. Relative CBF and BOLD measured during hypercapnia are used to calculate M (the theoretical ceiling of BOLD signal change), which can be combined with relative CBF and BOLD measured during the visual task to calculate relative $CMRO_2$ (and NVC ratio). (B) Each tier of the neural-glial-vascular model can be represented by one measure: $CMRO_2$ (tier I) represents neurometabolic activity, CBF (tier III) represents vascular responses to changes in that activity, and the NVC ratio (tier II) represents the intermediaries that link blood flow and metabolism.

negligible $CMRO_2$ change (but see Zappe et al. 2008; Xu et al. 2011; Thesen et al. 2012). ROI-level PSC estimates for both modalities (BOLD and CBF) during hypercapnia were used to calculate the M value for each participant's visual cortex using a modified form of Equation (1):

$$M = \frac{\frac{\Delta BOLD}{BOLD_0}}{\left(1-\left(\frac{CBF}{CBF_0}\right)^{\alpha-\beta}\right)} \quad (2)$$

After regional M values were calculated from hypercapnic calibration data, $CMRO_2$ change was calculated from BOLD PSC and CBF changes evoked during performance of the visual task using another modified form of Equation (1) that has been solved for $CMRO_2$:

$$\frac{CMRO_2}{CMRO_{2|0}} = \left(1 - \frac{\frac{\Delta BOLD}{BOLD_0}}{M}\right)^{1/\beta} \left(\frac{CBF}{CBF_0}\right)^{1-\alpha/\beta} \quad (3)$$

The NVC ratio, relating stimulus-evoked CBF to stimulus-evoked $CMRO_2$, can be calculated by dividing CBF PSC by $CMRO_2$ PSC. Thus, the NVC ratio represents the relative amount of stimulus-evoked CBF change in response to a given unit change in $CMRO_2$. However, the quotients of CBF PSC and $CMRO_2$ PSC have inordinately high variance, acting similarly to a Cauchy random variable (Cassela and Berger 2002), making them, by definition, highly inefficient estimators of the NVC ratio. We instead chose an approach used previously (Kim et al. 1999; Hoge et al. 1999a, 1999b; Wey et al. 2011) to quantify the NVC ratio with much lower variance for a given group and condition using the parameter estimates from a GLM that predicts $CMRO_2$ from CBF. Using this method, the NVC ratio is the reciprocal of the regression parameter estimate produced by this GLM fit by ordinary least squares. Using a first-order approximation (Wolter 2007), the variance of the reciprocal of the parameter estimate from the GLM predicting $CMRO_2$ from CBF is given by Equation (4):

$$\mathrm{Var}\left(\frac{1}{\hat{\theta}}\right) \approx \left(\frac{1}{\hat{\theta}^2}\right)^2 \times \mathrm{Var}\left(\hat{\theta}\right) \quad (4)$$

Quality assurance

Eleven participants were excluded from subsequent analyses due to data quality. One younger participant was excluded for noncompliance. One older participant was later determined to have been diagnosed with sleep apnea (and thus may have had altered sensitivity to CO_2). One younger participant was excluded for having an outlier M-value (>10 SDs from both the mean of the group and the entire sample). Three participants (2 young and 1 old) were excluded for having negative baseline CBF values, which led to large negative or incalculable $CMRO_2$ values. Three older participants were excluded for excessive head motion (in each case, rotation about the x-axis was >3°). One younger participant was excluded for aliasing artifacts on the MPRAGE structural image. Finally, 1 older participant was excluded due to failures of cortical parcellation and reconstruction during Freesurfer processing.

Results

Behavioral performance

Younger adults and older adults showed comparable performance on the in-scanner fixation task, confirming visual fixation and attention across groups. Formal tests of an age-group difference in reaction time (RT) using an independent-samples t-test revealed that younger adults ($M_Y = 728.20$ ms, $SEM_Y = 72.39$ ms) and older adults ($M_O = 741.03$ ms, $SEM_O = 85.03$ ms) did not differ significantly in RT on the visual attention task, $t(58) = 0.152$ ($P = 0.880$). Similar tests for group differences in accuracy rates on the task revealed that younger adults ($M_Y = 83.08\%$) and older adults ($M_O = 82.30\%$) did not differ significantly in accuracy, $t(58) = 0.261$ ($P = 0.794$).

Age differences in cortical volume

Prior to analysis of functional neurophysiologic data, we assessed whether there were significant differences in the volume of occipital cortex between age-groups. Group means of voxel counts within occipital lobe as defined by cortical parcellation in Freesurfer were numerically similar, and a formal test of significance (independent-samples t-test) revealed that younger ($M_Y = 87{,}819$ mm^3, $SEM_Y = 2339$ mm^3) and older adults ($M_O = 86{,}521$ mm^3, $SEM_O = 2088$ mm^3) did not differ significantly in the volume of occipital cortex, $t(58) = 0.403$ ($P = 0.689$).

Effects of age on BOLD, blood flow, oxygen metabolism, and NVC

In the focal region of visual cortex most stimulated by the flickering checkerboard, represented by the 5,000 mm^3 with highest signal, we observed greater BOLD signal in younger relative to older adults across stimulus frequency conditions, $F(1, 47) = 11.450$ ($P = 0.001$; see Fig. 4). Conversely, we observed greater $CMRO_2$ in older compared to younger adults across stimulus frequency conditions, $F(1, 47) = 7.018$ ($P = 0.011$). There was no significant difference in relative CBF between younger and older adults, $F(1, 47) = 0.781$ ($P = 0.381$). These results replicate previous findings from our lab (Hutchison, Lu, et al. 2013; Hutchison, Shokri-Kojori, et al. 2013).

Calculation of $CMRO_2$ depends critically upon the calibration constant M (see Materials and methods), the theoretical maximum change in BOLD signal. M is known to vary not only across participants but also across cortical regions and even from 1 scanning session to another (Leontiev et al. 2007; Bright et al. 2019). Age-related differences in M would have important consequences for the assessment of age-related differences in $CMRO_2$ (and thus also in NVC ratio). Inspection of Table 1 suggests that differences in M are minimal between younger ($M_Y = 9.492$, $SD_Y = 2.606$) and older adults ($M_O = 10.722$, $SD_O = 2.946$). To assess whether these differences in M could influence the estimation of age-group differences in $CMRO_2$, we formally tested for age-group differences in M using an independent-samples t-test. There was no significant age-group difference in M, $t(47) = 1.477$ ($P = 0.146$).

We observed that the NVC ratio was higher in younger than in older adults across all conditions (see Fig. 4). An independent samples t-test revealed that the NVC ratio

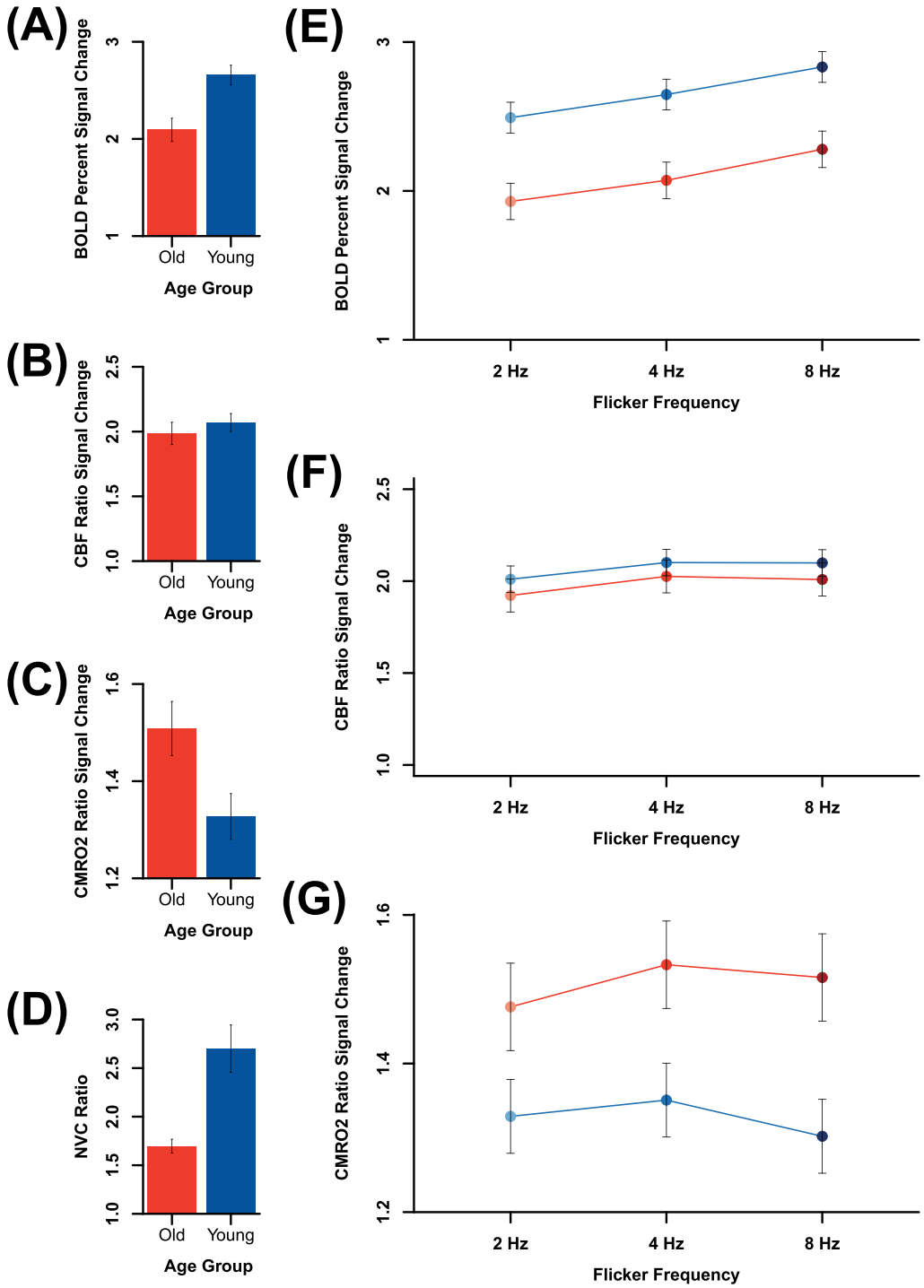

Fig. 4. Main effects of age-group on (A) BOLD, (B) relative CBF, (C) relative $CMRO_2$, and (D) NVC ratio, main effects of flicker frequency, and age-group × flicker frequency interaction effects on (E) BOLD, (F) relative CBF, and (G) relative $CMRO_2$. Both (A) BOLD and (D) NVC ratio were significantly higher in younger than in older adults, whereas relative (C) $CMRO_2$ was significantly higher in older than in younger adults, and no group difference was observed in (B) relative CBF. The effects of flicker frequency on both (E) BOLD and (F) relative CBF were significant, and the quadratic main effect of flicker frequency was significant on (G) relative $CMRO_2$. The only significant age-group × flicker frequency interaction effect was observed in NVC ratio (see Fig. 5B, top row).

was significantly higher in younger than in older adults, $t(47) = 4.027$ ($P = 2.044 \times 10^{-4}$).

When examining the neurophysiologic measures in the focal region of visual cortex, no age-group × flicker frequency interaction effects were significant for BOLD ($d = 0.018$), relative CBF ($d = 0.145$), or relative $CMRO_2$ ($d = 0.252$). Effectively, the nature of the change in measured signal with flicker frequency did not depend on age-group for these quantities. The mixed-effects linear model did reveal a significant age-group × flicker

Table 1. Group means and SDs of *M* and quantities used in the *M* calculation.

Quantity	Mean, younger group	SD, younger group	Mean, older group	SD, older group
BOLD PSC (hypercapnia)	9.012	2.545	10.273	2.707
CBF PSC (hypercapnia)	25.134	15.098	26.821	11.706
M (%)	9.492	2.606	10.722	2.946

Table 2. Age-group × flicker frequency interaction effect on NVC ratio by mask size, including results of individual t-contrasts between 2 Hz versus 4 Hz and 2 Hz versus 8 Hz conditions.

Region of occipital lobe	F-score ($df = 2, 86$)	*P*-value	*t*-score, 2 Hz versus 4 Hz ($df = 86$)	*P*-value	*t*-score, 2 Hz versus 8 Hz ($df = 86$)	*P*-value
Focal (innermost 5,000 mm^3)	9.325	$\mathbf{2.160 \times 10^{-4}}$	2.295	$\mathbf{2.415 \times 10^{-2}}$	4.317	$\mathbf{4.216 \times 10^{-5}}$
Proximal (surrounding 5,000 mm^3)	3.781	$\mathbf{2.668 \times 10^{-2}}$	1.029	$\mathbf{3.065 \times 10^{-3}}$	2.712	$\mathbf{8.071 \times 10^{-3}}$
Distal (outermost 10,000 mm^3)	1.526	2.232×10^{-1}	0.980	3.298×10^{-1}	1.746	8.441×10^{-1}

Note. Bolded *P*-values represent significant results.

frequency interaction effect on the NVC ratio in the focal ROI (see Table 2 and Fig. 5; see also Supplemental Information).

Analysis of focal, proximal, and distal regional signal differences

To assess the spatial distribution of flicker frequency effects on NVC, and whether those effects varied with age, we compared NVC ratios from the focal ROI to NVC ratios from nonoverlapping concentric ROIs. Discrete volumes of visual cortex that shared a geometric center with the Focal ROI were chosen to be included for analysis. These volumes were labeled as the proximal ROI (the top 10,000 mm^3 excluding the focal ROI) and the distal ROI (the top 20,000 mm^3 excluding the proximal and focal ROIs). Significant interaction effects were not observed in more outlying ROIs (i.e. 30,000 and 40,000 mm^3), although significant age main-effects remained. Representative masks are depicted in Fig. 5A.

Greater NVC ratio in younger relative to older adults across stimulus frequency conditions was observed at all volumes. This main effect of age-group was significant at all mask sizes. Additionally, the NVC ratio in the 4 and 8 Hz conditions was higher than in the 2 Hz condition in younger adults in all mask sizes, but the NVC ratio did not appear to change with condition in older adults at any mask size. Importantly, a formal test of significance revealed that the age-group × flicker frequency interaction effect was significant in the focal (Cohen's $d = 1.67$) and proximal ($d = 1.11$) ROIs but not in the distal ROI (see Table 2 and Fig. 5).

The parameters α and β are fundamental in the calculation of $CMRO_2$ using the deoxyhemoglobin dilution model and thus in calculation of the NVC ratio. α represents the nonlinear coupling between CBF and CBV (Grubb Jr. et al. 1974; Chen and Pike 2009), whereas β represents features of the anatomy of microvasculature (Bright et al. 2019) and depends on the standing magnetic field strength. Although work investigating age-group differences in these parameters remains to be done, it is supposable that such differences may develop with age. To investigate the potential influences of age-group differences in these parameters upon our results, we conducted sensitivity analyses, wherein we recalculated *M* and $CMRO_2$ values while varying both α and β between extremes of values reported previously in the calibrated fMRI literature (Grubb Jr. et al. 1974; Pasley et al. 2007; Chen and Pike 2009; Mohtasib et al. 2012). Results of these analyses indicated that our result of a significant age-group × flicker frequency interaction effect was robust to group-equivalent and group-independent variation in α and β (see Supplemental Information for more detail).

A substantial gap exists in calibrated fMRI studies of aging in that no prior studies have empirically tested for age-group differences in α and β. Mohtasib et al. (2012) did simulate the effects of such differences, positing that, across the lifespan, α would slowly increase (at a rate of half a percent per year), while β would decrease at the same rate. However, it is important to note that this rate was extrapolated from a single result showing age-reductions in gray-matter perfusion (Parkes et al. 2004). As discussed above, the relationships between α and β to BOLD and $CMRO_2$ are complex, both mathematically (acting in nonlinear fashion) and conceptually (representing very specific physical or physiologic relationships), and as such, while both quantities probably vary with age, more work is required to determine the precise fashion in which α and β change over the lifespan.

Discussion

Using a dual-echo calibrated fMRI approach, we separated the BOLD signal into its neurophysiologic constituents of CBF and $CMRO_2$ to examine the NVC ratio, and we assessed the separate and combined effects

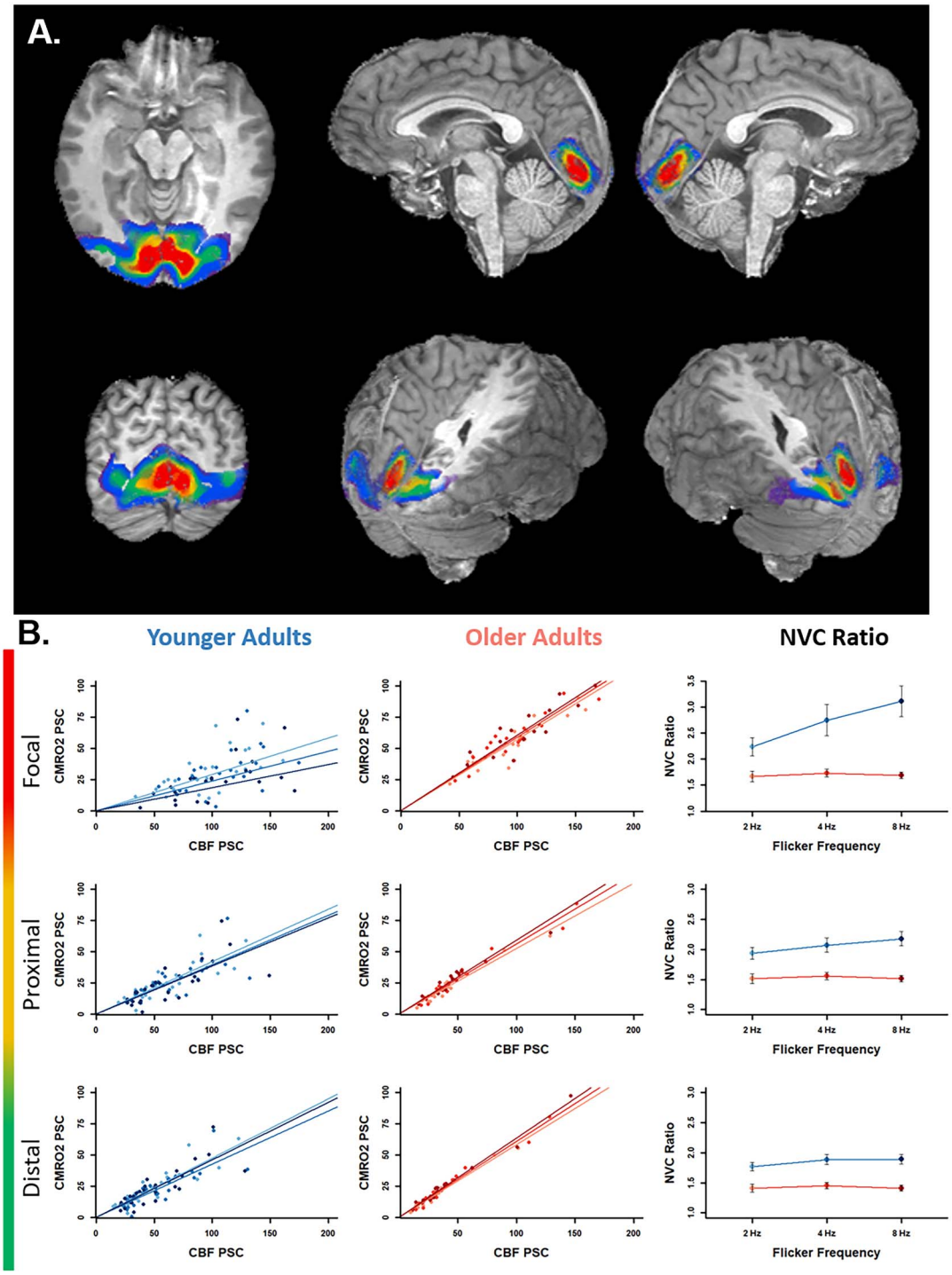

Fig. 5. A) ROIs from a representative participant. Colors indicate the size of the maximum extent of the ROI: Focal (red; 5,000 mm^3), proximal (yellow; 10,000 mm^3), and distal (green; 20,000 mm^3). Also depicted for reference are more outlying ROIs in blue (30,000 mm^3) and purple (40,000 mm^3). B) The first 2 columns depict PSC values of $CMRO_2$ by CBF for each frequency in younger (left) and older (center) adults, and the right column depicts the NVC ratio for each group at each frequency, calculated as the reciprocals of the by-condition parameter estimates from the left two columns. Each row depicts results for each of the focal (top), proximal (middle), and distal (bottom) regions corresponding to representative ROIs above in red, yellow, and green, respectively. Results for younger adults are represented in blue, and those for older adults are represented in red. Lighter and darker shades represent lower and higher frequency conditions, respectively. Error bars in the right column represent the extent to which individual observations vary from the least-squares regression line in the left and center columns for younger and older adults, respectively, and were calculated using Equation (4) (see Materials and methods). Greater variability was observed in younger adults.

of age and modulations in demand on NVC in the visual system. Results from this approach yielded 3 key findings. First, in response to flickering checkerboard stimuli, we observed reduced BOLD response with age across primary visual cortex, together with age-group equivalent blood flow responses and age-increases in oxygen metabolism, resulting in overall lower NVC ratios in older than in younger adults. These results replicate earlier results from our laboratories (Hutchison, Lu, et al. 2013; Hutchison, Shokri-Kojori, et al. 2013)

and support a growing body of evidence in animal (e.g. Grosche et al. 2013; Jessen et al. 2017; Tarantini et al. 2017, 2021; Yabluchanskiy et al. 2021) and human studies (Howarth et al. 2021; Hutchison, Lu, et al. 2013; Hutchison, Shokri-Kojori, et al. 2013; Tsvetanov et al. 2021), showing that NVC is disrupted in aging. Second, analysis of BOLD and its physiologic constituents (i.e. changes in blood flow and oxygen metabolism) at multiple frequencies indicated that NVC was sensitive to the modulation of visual system demand in younger adults but was insensitive to demand in older adults. Previous work has shown that the intact NVC system of healthy younger adults is responsive to variations in stimulus characteristics (e.g. intensity, duration; Leontiev et al. 2007; Lin et al. 2009, 2010; Moradi et al. 2012; Liang et al. 2013; Moradi and Buxton 2013; Buxton et al. 2014; Mark et al. 2015). Results observed here demonstrate that the NVC system is also responsive to variations in stimulus frequency in younger but not in older adults. Third, while the NVC ratio was greater in younger than older adults throughout the primary visual cortex, the sensitivity of NVC in younger adults to stimulus characteristics was limited to the focal regions of visual cortex. These results are congruent with murine and primate studies demonstrating the deleterious effects of aging upon the systems that subserve NVC (Peters and Sethares 2004; Tarantini et al. 2017).

The combination of our blood-flow change measurements and BOLD signal, together with the hypercapnia calibration experiment, permitted us to calculate both the rate of oxygen metabolism and the NVC ratio within brain parenchyma and to assess age-group differences in these quantities. In the focal ROI, we observed age-equivalent stimulus-evoked blood flow together with age-related increases in stimulus-evoked oxygen metabolism. These patterns explain both the higher BOLD signal and the higher NVC ratio (i.e. the change in blood flow per unit change in oxygen metabolism) observed in younger relative to older adults. The greater oxygen metabolism we observed in older adults would not be explained by observations of age-increases in baseline oxygen metabolism in prior work (Lu et al. 2011), as such an elevated baseline would yield the opposite result (i.e. greater oxygen metabolism in younger than in older adults). Rather, our result of age-decreases in BOLD signal reflects age-differential increases in stimulus-evoked oxygen metabolism together with age-equivalence in stimulus-evoked blood flow (cf. Ross et al. 1997). Further, physiologic studies present compelling evidence that the metabolic rate of oxygen in brain tissue actually increases in the presence of restricted O_2 availability (Harik et al. 1995; Hochachka et al. 1994; Richards et al. 2007; Smith et al. 2013; Xu et al. 2012). These observations in the focal ROI replicate prior research from our laboratories (Hutchison, Lu, et al. 2013; Hutchison, Shokri-Kojori, et al. 2013) in a larger sample using a similar task.

The calibrated fMRI method permitted us to assess the neural and vascular phenomena underlying age-related changes in BOLD signal. Change in BOLD signal over time, known as the hemodynamic response function (HRF), has been used extensively in the study of both healthy (e.g. Rypma and D'Esposito 2000; Rypma et al. 2001; Cabeza 2002; Reuter-Lorenz 2002; Aizenstein et al. 2004; Hedden and Gabrieli 2004; Rypma et al. 2006; Fabiani et al. 2014; Thomas et al. 2014) and pathological aging of the brain (e.g. Machulda et al. 2003; Hao et al. 2005; Rombouts et al. 2005; Cole et al. 2006; Goekoop et al. 2004; Hämäläinen et al. 2007). The HRF features a reliable time-course (over a range of 15–30 s following stimulus) and regular shape in healthy, young adults, though regional and interindividual variability has been observed (Aguirre et al. 1998; Miezin et al. 2000; Handwerker et al. 2004). Study of age-group differences in shape parameters of this function have shown significant age-related increases in variability (D'Esposito et al. 1999, 2003; Handwerker et al. 2007; Tsvetanov et al. 2015, 2019; Abdelkarim et al. 2019; Turner, Fischer, et al. 2019; West et al. 2019). The age-related reductions in NVC we observed in this study provide a plausible mechanism for this increased variability. Disruption in the delivery of oxygen (and other metabolites) in the context of the increased neurometabolic activity that we observed in older adults would be expected to alter processes underlying the HRF. For instance, shape parameters reflecting the timing of hemodynamic activity (e.g. time-to-peak and time-to-trough; Turner, Hubbard et al. 2019) which have been observed to increase with age (West et al. 2019) could reflect restrictions in the speed with which neural assemblies generate action potentials required for timely signal transmission, as has been observed in murine models of aging (e.g. Insel et al. 2012). Importantly, the age-reductions we observed in the NVC ratio do not reflect reduced neurometabolic activity in older adults. On the contrary, the reduced NVC ratio in older adults actually reflects disproportionate increases in stimulus-evoked neurometabolic activity (i.e. demand) which cannot be matched sufficiently by the blood flow response (i.e. supply). Such a desynchronization between blood supply and neurometabolic demand would lead to disruption of the homeostatic mechanisms necessary to maintain ionic gradients at resting potential (Abdelkarim et al. 2019), in turn limiting the frequency with which neural assemblies transmit signals reflected in age-related HRF shape changes.

Parametric modulation of the checkerboard flicker frequency (2, 4, and 8 Hz) revealed that the linear BOLD increases observed here, and also observed in many prior studies (e.g. Kwong et al. 1992; Thomas and Menon 1998; Zhu et al. 1998; Ozus et al. 2001; Hagenbeek et al. 2002; Pastor et al. 2003; Singh et al. 2003; Parkes et al. 2004; Cliff et al. 2013), result from complicated relationships between the physiologic components underlying the BOLD signal (i.e. stimulus-evoked blood flow and oxygen metabolism) and stimulus

frequency. While stimulus-evoked blood flow increases between 2 and 8 Hz, stimulus-evoked oxygen metabolism assumes a quadratic pattern, increasing from 2 to 4 Hz, but decreasing from 4 to 8 Hz. Previous studies investigating oxygen metabolism changes with flicker frequency in visual cortex have also identified such a $CMRO_2$ peak at 4 Hz (Zhu et al. 1998; Vafaee et al. 1999; Lin et al. 2010; see also Jessen et al. 2017). A study by Lin et al. (2010) also observed peak oxygen extraction fraction and ATP concentration at 8 Hz, suggesting a shift in the source metabolites utilized for ATP production at lower versus higher frequencies (i.e. aerobic metabolism at lower frequencies and anaerobic glycolysis at higher frequencies). More work is certainly needed to understand the complexities underlying the apparently straightforward monotonic increases in BOLD signal with increasing frequency and possibly cognitive demand (e.g. Rypma et al. 1999; Cappell et al. 2010; see also Csipo et al. 2021).

The introduction of stimulus frequency into a study of the effects of aging allowed us to test for interactions between the effects of stimulus frequency and age-group. Within the focal ROI, no such interaction effects were observed for BOLD signal, stimulus-evoked blood flow, or stimulus-evoked oxygen metabolism, but a significant interaction was observed for the NVC ratio. Interestingly, this interaction effect was attenuated in more distal ROIs (outside the metabolic focal point). In other words, the frequency dependence of stimulus-induced change in blood flow per unit change in oxygen metabolism was different for younger and older adults. In younger adults, the NVC ratio actually increased with increasing frequency; similar changes in NVC ratio with varying stimulus properties have been reported previously for both visual (e.g. Moradi et al. 2012; Liang et al. 2013) and cognitive (Csipo et al. 2021) stimuli. By contrast, for older adults, the NVC ratio remained relatively unchanged with increasing frequency.

NVC increases with increasing frequency could serve to regulate oxygen delivery mechanisms (Hyder et al. 1998; Hudetz 1999; Lin et al. 2010; Celaya-Alcala et al. 2021) as metabolic demand increases. Effective preservation of oxygen delivery to tissue is a critical homeostatic process because very little oxygen is available to neurons and glia that require it from sources other than erythrocytes flowing through the vasculature (Hyder et al. 1998; Buxton 2010). Successful maintenance of tissue oxygen availability could require additional vascular support from the immediately surrounding areas of cortex in younger adults. Such a vascular support network that extends beyond immediate regions of active tissue has been observed in other studies (e.g. West et al. 2021). Age-related disruptions to the NVC system would result in mismatches between not only stimulus-evoked blood flow and stimulus-evoked oxygen metabolism but also in mismatches between oxygen extraction, which could result in failures to maintain oxygen delivery due to diminished vascular support in cortical areas immediately surrounding the focal regions of neurometabolic activity (cf. Hubbard et al. 2021). Future studies that include the collection of hyperoxia data will be necessary to more directly examine the role of tissue oxygen delivery in NVC differences between age-groups.

In contrast to our finding that NVC sensitivity to stimulus frequency in younger adults is specific to the center of neurometabolic activity, we observed overall age-differences in the NVC ratio which persisted throughout visual cortex. Based on murine models of astrocyte function in NVC (Haydon and Carmignoto 2006; Carmignoto and Gómez-Gonzalo 2010; Petzold and Murthy 2011; Otsu et al. 2015), we hypothesize that the spatially persistent NVC age main-effects might reflect brain-wide structural and functional changes to astrocytes (Figley and Stroman, 2011; Tarantini et al. 2017; Howarth et al. 2017) that pervade the aging brain. Such changes include astrocyte hypertrophy (Rodríguez-Arellano et al. 2016), loss of endfoot domain specificity (Bors et al. 2018), and toxic reactivity (e.g. increased inflammatory signaling; see Abdelkarim et al. 2019). Reductions in cerebrovascular reactivity (CVR) do not account for this result (Taneja et al. 2020). Indeed, studies of CVR changes with age have found minimal age-differences in occipital cortex (Peng et al. 2018). More work is certainly needed to explicitly test this hypothesis. Work underway in our laboratories is examining the specific nature of individual NVC components and how they contribute to the phenomena we observed here.

We observed age-related increases in stimulus-evoked oxygen metabolism, similar to previous studies (e.g. Lu et al. 2011; Hutchison, Lu, et al. 2013; Hutchison, Shokri-Kojori, et al. 2013; Jessen et al. 2017). The mechanisms underlying this phenomenon are not yet known. They may be related, however, to known decreases in ATP availability with age (for review, see Harper et al. 2004). Experimental work examining the relationship between ATP availability and oxygen metabolism remains to be done (but see Salin et al. 2015; Andersen et al. 2019). However, one possibility is that the neurometabolic system responds to this ATP deficit through increased aerobic metabolism (i.e. increased $CMRO_2$) to generate higher levels of ATP in mitochondria (Camandola and Mattson 2017). Despite these age-related increases in oxygen metabolism, however, ATP deficits persist. One mechanistic rationale for such mitochondrial inefficiency (i.e. producing less ATP per molecule of oxygen) might be to reduce the production of inflammatory reactive oxygen species byproducts (Brand 2000; Mookerjee et al. 2010). A second possibility involves the levels of oxygen available to neural tissue. Xu et al. (2012) found that manipulation of the fraction of inspired O_2 has a dose-dependent effect on brain oxygen metabolism. Their results showed that oxygen metabolism increases significantly during hypoxia but actually decreases during hyperoxia. Thus, a dearth of oxygen that may accumulate following supply–demand

mismatches by the NVC system may produce conditions wherein oxygen metabolism in older adults is actually higher. Irrespective of the mechanism, our results show that age-related increases in oxygen metabolism remain unmatched by blood flow responses, implicating glial intermediaries as points of failure within the aged neural-glial-vascular system.

Conclusion

In this study, we assessed age-differences in the effects of stimulus frequency on the NVC system in visual cortex. We observed age-equivalent stimulus-evoked blood flow (tier III of the neural-glial-vascular model) in the presence of greater stimulus-evoked oxygen metabolism (tier I of the neural-glial-vascular model) in older compared to younger adults. Measurement of these processes, via measurement of BOLD signal, permitted us to calculate the NVC ratio (i.e. the change in blood flow per unit change in oxygen metabolism). This NVC ratio (tier II of the neural-glial-vascular model) was reliably greater in younger than in older adults regardless of stimulus frequency or the volume of cortex over which it was measured. Moreover, blood flow increased disproportionately with stimulus-evoked metabolic increases (specifically within the center of neurometabolic activity) in younger but not in older adults. The age-related disruption of NVC that we observed rendered the older system unresponsive to increases in stimulus frequency. These results implicate the glial component of the neural-glial-vascular signaling system as a significant contributor to age-related decline in brain function.

Acknowledgments

The authors would like to thank Lindsey Michelle for assistance in figure creation and John Hart, Jr, for remarks on previous drafts of this manuscript.

Supplementary material

Supplementary material is available at *Cerebral Cortex Journal* online.

Funding

This work was supported by National Institute of Health grants (R01AG047972 to B.R. and H.L., R01AG029523 to B.R., R01NS106711 to H.L., R01NS106702 to H.L., F32MH114525 to N.A.H.; P20GM130461[6026] to N.A.H.), the Brain and Behavior Research Foundation and Vital Projects Investigator Fund, Inc. (N.A.H.), and the Nebraska Biomedical Research Development Funds (N.A.H.).

Data availability

The data that support the findings of this study are available from the corresponding author (BR) upon reasonable request.

Conflict of interest statement. None declared.

References

Abdelkarim D, Zhao Y, Turner MP, Sivakolundu DK, Lu H, Rypma B. A neural-vascular complex of age-related changes in the human brain: anatomy, physiology, and implications for neurocognitive aging. *Neurosci Biobehav Rev*. 2019:107:927–944.

Aguirre GK, Zarahn E, D'Esposito M. The variability of human, BOLD hemodynamic responses. *NeuroImage*. 1998:8(4):360–369.

Ainslie PN, Burgess KR. Cardiorespiratory and cerebrovascular responses to hyperoxic and hypoxic rebreathing: effects of acclimatization to high altitude. *Respir Physiol Neurobiol*. 2008: 161(2):201–209.

Aizenstein HJ, Clark KA, Butters MA, Cochran J, Stenger VA, Meltzer CC, Reynolds CF, Carter CS. The BOLD hemodynamic response in healthy aging. *J Cogn Neurosci*. 2004:16(5):786–793.

Alsop DC, Detre JA, Golay X, Günther M, Hendrikse J, Hernandez-Garcia L, Lu H, MacIntosh BJ, Parkes LM, Smits M, et al. Recommended implementation of arterial spin-labeled perfusion MRI for clinical applications: a consensus of the ISMRM perfusion study group and the European consortium for ASL in dementia. *Magn Reson Med*. 2015:73(1):102–116.

Ances BM, Liang CL, Leontiev O, Perthen JE, Fleisher AS, Lansing AE, Buxton RB. Effects of aging on cerebral blood flow, oxygen metabolism, and blood oxygenation level dependent responses to visual stimulation. *Hum Brain Mapp*. 2009:30(4):1120–1132.

Andersen JV, Jakobsen E, Waagepetersen HS, Aldana BI. Distinct differences in rates of oxygen consumption and ATP synthesis of regionally isolated non-synaptic mouse brain mitochondria. *J Neurosci Res*. 2019:97(8):961–974.

Aslan S, Xu F, Wang PL, Uh J, Yezhuvath US, Van Osch M, Lu H. Estimation of labeling efficiency in pseudocontinuous arterial spin labeling. *Magn Reson Med*. 2010:63(3):765–771.

Attwell D, Buchan AM, Charpak S, Lauritzen M, MacVicar BA, Newman EA. Glial and neuronal control of brain blood flow. *Nature*. 2010:468(7321):232–243.

Bennett IJ, Madden DJ. Disconnected aging: cerebral white matter integrity and age-related differences in cognition. *Neuroscience*. 2014:276:187–205.

Bennett IJ, Rypma B. Advances in functional neuroanatomy: a review of combined DTI and fMRI studies in healthy younger and older adults. *Neurosci Biobehav Rev*. 2013:37(7):1201–1210.

Bennett IJ, Madden DJ, Vaidya CJ, Howard DV, Howard JH Jr. Age-related differences in multiple measures of white matter integrity: a diffusion tensor imaging study of healthy aging. *Hum Brain Mapp*. 2010:31(3):378–390.

Birn RM, Cox RW, Bandettini PA. Detection versus estimation in event-related fMRI: choosing the optimal stimulus timing. *NeuroImage*. 2002:15(1):252–264.

Biswal B, Yetkin FZ, Haughton VM, Hyde JS. Functional connectivity in the motor cortex of resting human brain using echo-planar MRI. *Magn Reson Med*. 1995:34(4):537–541.

Bors L, Tóth K, Tóth EZ, Bajza Á, Csorba A, Szigeti K, Máthé D, Perlaki G, Orsi G, Tóth GK, et al. Age-dependent changes at the blood-brain barrier: a comparative structural and functional study in young adult and middle aged rats. *Brain Res Bull*. 2018:139: 269–277.

Brand MD. Uncoupling to survive? The role of mitochondrial inefficiency in ageing. *Exp Gerontol*. 2000:35(6–7):811–820.

Bright MG, Croal PL, Blockley NP, Bulte DP. Multiparametric measurement of cerebral physiology using calibrated fMRI. *NeuroImage*. 2019:187:128–144.

Bulte DP, Kelly M, Germuska M, Xie J, Chappell MA, Okell TW, Bright MG, Jezzard P. Quantitative measurement of cerebral physiology using respiratory-calibrated MRI. *NeuroImage*. 2012:60(1):582–591.

Buxton R. Interpreting oxygenation-based neuroimaging signals: the importance and the challenge of understanding brain oxygen metabolism. *Front Neuroenerg*. 2010:2:8.

Buxton RB, Griffeth VE, Simon AB, Moradi F. Variability of the coupling of blood flow and oxygen metabolism responses in the brain: a problem for interpreting BOLD studies but potentially a new window on the underlying neural activity. *Front Neurosci*. 2014:8:139.

Cabeza R. Hemispheric asymmetry reduction in older adults: the HAROLD model. *Psychol Aging*. 2002:17(1):85.

Cabeza R, Daselaar SM, Dolcos F, Prince SE, Budde M, Nyberg L. Task-independent and task-specific age effects on brain activity during working memory, visual attention and episodic retrieval. *Cereb Cortex*. 2004:14(4):364–375.

Camandola S, Mattson MP. Brain metabolism in health, aging, and neurodegeneration. *EMBO J*. 2017:36(11):1474–1492.

Cappell KA, Gmeindl L, Reuter-Lorenz PA. Age differences in prefontal recruitment during verbal working memory maintenance depend on memory load. *Cortex*. 2010:46(4):462–473.

Carmignoto G, Gómez-Gonzalo M. The contribution of astrocyte signalling to neurovascular coupling. *Brain Res Rev*. 2010:63(1–2): 138–148.

Casella G, Berger RL. *Statistical inference*. Pacific Grove (CA): Duxbury; 2002

Cauli B, Hamel E. Brain perfusion and astrocytes. *Trends Neurosci*. 2018:41(7):409–413.

Celaya-Alcala JT, Lee GV, Smith AF, Li B, Sakadžic S, Boas DA, Secomb TW. Simulation of oxygen transport and estimation of tissue perfusion in extensive microvascular networks: Application to cerebral cortex. *J Cereb Blood Flow Metab*. 2021:41(3):656–669.

Chandran R, Kumar M, Kesavan L, Jacob RS, Gunasekaran S, Lakshmi S, Sadasivan C, Omkumar RV. Cellular calcium signaling in the aging brain. *J Chem Neuroanat*. 2019:95:95–114.

Chen JJ, Pike GB. BOLD-specific cerebral blood volume and blood flow changes during neuronal activation in humans. *NMR Biomed*. 2009:22(10):1054–1062.

Chen BR, Kozberg MG, Bouchard MB, Shaik MA, Hillman EM. A critical role for the vascular endothelium in functional neurovascular coupling in the brain. *J Am Heart Assoc*. 2014:3(3): e000787.

Chiarelli PA, Bulte DP, Gallichan D, Piechnik SK, Wise R, Jezzard P. Flow-metabolism coupling in human visual, motor, and supplementary motor areas assessed by magnetic resonance imaging. *Magn Reson Med*. 2007:57(3):538–547.

Cliff M, Joyce DW, Lamar M, Dannhauser T, Tracy DK, Shergill SS. Aging effects on functional auditory and visual processing using fMRI with variable sensory loading. *Cortex*. 2013:49(5): 1304–1313.

Cole LJ, Farrell MJ, Duff EP, Barber JB, Egan GF, Gibson SJ. Pain sensitivity and fMRI pain-related brain activity in Alzheimer's disease. *Brain*. 2006:129(11):2957–2965.

Csipo T, Lipecz A, Mukli P, Bahadli D, Abdulhussein O, Owens CD, Tarantini S, Hand RA, Yabluchanska V, Kellawan JM, et al. Increased cognitive workload evokes greater neurovascular coupling responses in healthy young adults. *PLoS One*. 2021:16(5): e0250043.

Dalkara T, Gursoy-Ozdemir Y, Yemisci M. Brain microvascular pericytes in health and disease. *Acta Neuropathol*. 2011:122(1): 1–9.

Davis TL, Kwong KK, Weisskoff RM, Rosen BR. Calibrated functional MRI: mapping the dynamics of oxidative metabolism. *Proc Natl Acad Sci*. 1998:95(4):1834–1839.

Desikan RS, Ségonne F, Fischl B, Quinn BT, Dickerson BC, Blacker D, Buckner RL, Dale AM, Maguire RP, Hyman BT, et al. An automated labeling system for subdividing the human cerebral cortex on MRI scans into gyral based regions of interest. *NeuroImage*. 2006:31(3):968–980.

D'Esposito M, Zarahn E, Aguirre GK, Rypma B. The effect of normal aging on the coupling of neural activity to the bold hemodynamic response. *NeuroImage*. 1999:10(1):6–14.

D'Esposito M, Deouell LY, Gazzaley A. Alterations in the BOLD fMRI signal with ageing and disease: a challenge for neuroimaging. *Nat Rev Neurosci*. 2003:4(11):863–872.

Fabiani M, Gordon BA, Maclin EL, Pearson MA, Brumback-Peltz CR, Low KA, McAuley E, Sutton BP, Kramer AF, Gratton G. Neurovascular coupling in normal aging: a combined optical, ERP and fMRI study. *NeuroImage*. 2014:85:592–607.

Figley CR, Stroman PW. The role(s) of astrocytes and astrocyte activity in neurometabolism, neurovascular coupling, and the production of functional neuroimaging signals. *Eur J Neurosci*. 2011:33(4):577–588.

Fischl B. FreeSurfer. *NeuroImage*. 2012:62(2):774–781.

Friston KJ, Penny WD, Glaser DE. Conjunction revisited. *NeuroImage*. 2005:25(3):661–667.

Goekoop R, Rombouts SARB, Jonker C, Hibbel A, Knol DL, Truyen L, Barkhof F, Scheltens P. Challenging the cholinergic system in mild cognitive impairment: a pharmacological fMRI study. *NeuroImage*. 2004:23(4):1450–1459.

Gottfried C, Tramontina F, Gonçalves D, Gonçalves CA, Moriguchi E, Dias RD, Wofchuk ST, Souza DO. Glutamate uptake in cultured astrocytes depends on age: a study about the effect of guanosine and the sensitivity to oxidative stress induced by H_2O_2. *Mech Ageing Dev*. 2002:123(10):1333–1340.

Griffeth VE, Buxton RB. A theoretical framework for estimating cerebral oxygen metabolism changes using the calibrated-BOLD method: modeling the effects of blood volume distribution, hematocrit, oxygen extraction fraction, and tissue signal properties on the BOLD signal. *NeuroImage*. 2011:58(1):198–212.

Griffeth VE, Perthen JE, Buxton RB. Prospects for quantitative fMRI: investigating the effects of caffeine on baseline oxygen metabolism and the response to a visual stimulus in humans. *NeuroImage*. 2011:57:809–816.

Grosche A, Grosche J, Tackenberg M, Scheller D, Gerstner G, Gumprecht A, Pannicke T, Hirrlinger PG, Wilhelmsson U, Hüttmann K, et al. Versatile and simple approach to determine astrocyte territories in mouse neocortex and hippocampus. *PLoS One*. 2013:8(7):e69143.

Grubb RL Jr, Raichle ME, Eichling JO, Ter-Pogossian MM. The effects of changes in PaCO2 cerebral blood volume, blood flow, and vascular mean transit time. *Stroke*. 1974:5(5):630–639.

Gu X, Chen W, Volkow ND, Koretsky AP, Du C, Pan Y. Synchronized astrocytic Ca2+ responses in neurovascular coupling during somatosensory stimulation and for the resting state. *Cell Rep*. 2018:23(13):3878–3890.

Hagenbeek RE, Rombouts SA, van Dijk BW, Barkhof F. Determination of individual stimulus-response curves in the visual cortex. *Hum Brain Mapp*. 2002:17(4):244–250.

Hämäläinen A, Pihlajamäki M, Tanila H, Hänninen T, Niskanen E, Tervo S, Karjalainen PA, Vanninen RL, Soininen H. Increased fMRI responses during encoding in mild cognitive impairment. *Neurobiol Aging*. 2007:28(12):1889–1903.

Handwerker DA, Ollinger JM, D'Esposito M. Variation of BOLD hemodynamic responses across subjects and brain regions and their effects on statistical analyses. *NeuroImage*. 2004:21(4):1639–1651.

Handwerker DA, Gazzaley A, Inglis BA, D'Esposito M. Reducing vascular variability of fMRI data across aging populations using a breathholding task. *Hum Brain Mapp*. 2007:28(9):846–859.

Hao J, Li K, Li K, Zhang D, Wang W, Yang Y, Yan B, Shan B, Zhou X. Visual attention deficits in Alzheimer's disease: an fMRI study. *Neurosci Lett*. 2005:385(1):18–23.

Harik SI, Lust WD, Jones SC, Lauro KL, Pundik S, LaManna JC. Brain glucose metabolism in hypobaric hypoxia. *J Appl Physiol*. 1995:79(1):136–140.

Harper ME, Bevilacqua L, Hagopian K, Weindruch R, Ramsey JJ. Ageing, oxidative stress, and mitochondrial uncoupling. *Acta Physiol Scand*. 2004:182(4):321–331.

Haydon PG, Carmignoto G. Astrocyte control of synaptic transmission and neurovascular coupling. *Physiol Rev*. 2006:86(3): 1009–1031.

Hedden T, Gabrieli JD. Insights into the ageing mind: a view from cognitive neuroscience. *Nat Rev Neurosci*. 2004:5(2):87–96.

Hillman EM. Coupling mechanism and significance of the BOLD signal: a status report. *Annu Rev Neurosci*. 2014:37:161–181.

Hochachka PW, Clark CM, Brown WD, Stanley C, Stone CK, Nickles RJ, Zhu GG, Allen PS, Holden JE. The brain at high altitude: hypometabolism as a defense against chronic hypoxia? *J Cereb Blood Flow Metab*. 1994:14(4):671–679.

Hoge RD. Calibrated fMRI. *NeuroImage*. 2012:62(2):930–937.

Hoge RD, Atkinson J, Gill B, Crelier GR, Marrett S, Pike GB. Investigation of BOLD signal dependence on cerebral blood flow and oxygen consumption: the deoxyhemoglobin dilution model. *Magn Reson Med*. 1999a:42(5):849–863.

Hoge RD, Atkinson J, Gill B, Crelier GR, Marrett S, Pike GB. Linear coupling between cerebral blood flow and oxygen consumption in activated human cortex. *Proc Natl Acad Sci*. 1999b:96(16): 9403–9408.

Howarth C, Sutherland BA, Choi HB, Martin C, Lind BL, Khennouf L, LeDue JM, Pakan JMP, Ko RWY, Ellis-Davies G, et al. A critical role for astrocytes in hypercapnic vasodilation in brain. *J Neurosci*. 2017:37(9):2403–2414.

Howarth C, Mishra A, Hall CN More than just summed neuronal activity: how multiple cell types shape the BOLD response. *Phil Trans Royal Soc B*. 2021:376(1815):20190630.

Hubbard NA, Turner MP, Ouyang M, Himes L, Thomas BP, Hutchison JL, Faghihahmadabadi S, Davis SL, Strain JF, Spence J, et al. Calibrated imaging reveals altered grey matter metabolism related to white matter microstructure and symptom severity in multiple sclerosis. *Hum Brain Mapp*. 2017:38(11):5375–5390.

Hubbard NA, Turner MP, Sitek KR, West KL, Kaczmarzyk JR, Himes L, Thomas BP, Lu H, Rypma B. Resting cerebral oxygen metabolism exhibits archetypal network features. *Hum Brain Mapp*. 2021: in press.

Hudetz AG. Mathematical model of oxygen transport in the cerebral cortex. *Brain Res*. 1999:817(1–2):75–83.

Hutchison JL, Lu H, Rypma B. Neural mechanisms of age-related slowing: the ΔCBF/ΔCMRO2 ratio mediates age-differences in BOLD signal and human performance. *Cereb Cortex*. 2013:23(10): 2337–2346.

Hutchison JL, Shokri-Kojori E, Lu H, Rypma B. A BOLD perspective on age-related neurometabolic-flow coupling and neural efficiency changes in human visual cortex. *Front Psychol*. 2013:4:244.

Hyder F, Shulman RG, Rothman DL. A model for the regulation of cerebral oxygen delivery. *J Appl Physiol*. 1998:85(2):554–564.

Hyder F. Neuroimaging with calibrated FMRI. *Stroke*. 2004:35(11): 2635–2641.

Insel N, Patron LA, Hoang LT, Nematollahi S, Schimanski LA, Lipa P, Barnes CA. Reduced gamma frequency in the medial frontal cortex of aged rats during behavior and rest: implications for age-related behavioral slowing. *J Neurosci*. 2012:32(46):16331–16344.

Jessen SB, Mathiesen C, Lind BL, Lauritzen M. Interneuron deficit associates attenuated network synchronization to mismatch of energy supply and demand in aging mouse brains. *Cereb Cortex*. 2017:27(1):646–659.

Jiang T, Cadenas E. Astrocytic metabolic and inflammatory changes as a function of age. *Aging Cell*. 2014:13(6):1059–1067.

Jukkola P, Guerrero T, Gray V, Gu C. Astrocytes differentially respond to inflammatory autoimmune insults and imbalances of neural activity. *Acta Neuropathol Commun*. 2013:1(1):70.

Kim SG, Rostrup E, Larsson HB, Ogawa S, Paulson OB. Determination of relative $CMRO_2$ from CBF and BOLD changes: significant increase of oxygen consumption rate during visual stimulation. *Magn Reson Med*. 1999:41(6):1152–1161.

Kohn JC, Lampi MC, Reinhart-King CA. Age-related vascular stiffening: causes and consequences. *Front Genet*. 2015:6:112.

Krueger M, Bechmann I. CNS pericytes: concepts, misconceptions, and a way out. *Glia*. 2010:58(1):1–10.

Kwong KK, Belliveau JW, Chesler DA, Goldberg IE, Weisskoff RM, Poncelet BP, Kennedy DN, Hoppel BE, Cohen MS, Turner R. Dynamic magnetic resonance imaging of human brain activity during primary sensory stimulation. *Proc Natl Acad Sci*. 1992:89(12): 5675–5679.

Lee Y, Morrison BM, Li Y, Lengacher S, Farah MH, Hoffman PN, Liu Y, Tsingalia A, Jin L, Zhang PW, et al. Oligodendroglia metabolically support axons and contribute to neurodegeneration. *Nature*. 2012:487(7408):443–448.

Le Bihan D, Turner R, Zeffiro TA, Cuenod CA, Jezzard P, Bonnerot V. Activation of human primary visual cortex during visual recall: a magnetic resonance imaging study. *Proc Natl Acad Sci*. 1993:90(24): 11802–11805.

Leontiev O, Dubowitz DJ, Buxton RB. $CBF/CMRO_2$ coupling measured with calibrated BOLD fMRI: sources of bias. *NeuroImage*. 2007:36(4):1110–1122.

Leutner S, Eckert A, Müller WE. ROS generation, lipid peroxidation and antioxidant enzyme activities in the aging brain. *J Neural Transm*. 2001:108(8–9):955–967.

Liang CL, Ances BM, Perthen JE, Moradi F, Liau J, Buracas GT, Hopkins SR, Buxton RB. Luminance contrast of a visual stimulus modulates the BOLD response more than the cerebral blood flow response in the human brain. *NeuroImage*. 2013:64:104–111.

Lin AL, Fox PT, Yang Y, Lu H, Tan LH, Gao JH. Time-dependent correlation of cerebral blood flow with oxygen metabolism in activated human visual cortex as measured by fMRI. *NeuroImage*. 2009:44(1):16–22.

Lin AL, Fox PT, Hardies J, Duong TQ, Gao JH. Nonlinear coupling between cerebral blood flow, oxygen consumption, and ATP production in human visual cortex. *Proc Natl Acad Sci*. 2010:107(18): 8446–8451.

Liu TT, Wong EC. A signal processing model for arterial spin labeling functional MRI. *NeuroImage*. 2005:24(1):207–215.

Lu H, van Zijl P. Experimental measurement of extravascular parenchymal BOLD effects and tissue oxygen extraction fractions using multi-echo VASO fMRI at 1.5 and 3.0 T. *Magn Reson Med*. 2005:53(4):808–816.

Lu H, Donahue MJ, Van Zijl PC. Detrimental effects of BOLD signal in arterial spin labeling fMRI at high field strength. *Magn Reson Med*. 2006:56(3):546–552.

Lu H, Xu F, Rodrigue KM, Kennedy KM, Cheng Y, Flicker B, Hebrank AC, Uh J, Park DC. Alterations in cerebral metabolic rate and blood supply across the adult lifespan. *Cereb Cortex*. 2011:21(6): 1426–1434.

Machulda MM, Ward HA, Borowski B, Gunter JL, Cha RH, O'Brien PC, Petersen RC, Boeve BF, Knopman D, Tang-Wai DF, et al. Comparison of memory fMRI response among normal, MCI, and Alzheimer's patients. *Neurology*. 2003:61(4):500–506.

MacVicar BA, Newman EA. Astrocyte regulation of blood flow in the brain. *Cold Spring Harb Perspect Biol*. 2015:7(5):a020388.

Mark CI, Mazerolle EL, Chen JJ. Metabolic and vascular origins of the BOLD effect: implications for imaging pathology and resting-state brain function. *J Magn Reson Imaging*. 2015:42(2): 231–246.

Metea MR, Newman EA. Glial cells dilate and constrict blood vessels: a mechanism of neurovascular coupling. *J Neurosci*. 2006:26(11): 2862–2870.

Miezin FM, Maccotta L, Ollinger JM, Petersen SE, Buckner RL. Characterizing the hemodynamic response: effects of presentation rate, sampling procedure, and the possibility of ordering brain activity based on relative timing. *NeuroImage*. 2000:11(6):735–759.

Mohtasib RS, Lumley G, Goodwin JA, Emsley HC, Sluming V, Parkes LM. Calibrated fMRI during a cognitive Stroop task reveals reduced metabolic response with increasing age. *NeuroImage*. 2012:59(2):1143–1151.

Mookerjee SA, Divakaruni AS, Jastroch M, Brand MD. Mitochondrial uncoupling and lifespan. *Mech Ageing Dev*. 2010:131(7–8):463–472.

Moradi F, Buxton RB. Adaptation of cerebral oxygen metabolism and blood flow and modulation of neurovascular coupling with prolonged stimulation in human visual cortex. *NeuroImage*. 2013:82:182–189.

Moradi F, Buračas GT, Buxton RB. Attention strongly increases oxygen metabolic response to stimulus in primary visual cortex. *NeuroImage*. 2012:59(1):601–607.

Ogawa S, Tank DW, Menon R, Ellermann JM, Kim SG, Merkle H, Ugurbil K. Intrinsic signal changes accompanying sensory stimulation: functional brain mapping with magnetic resonance imaging. *Proc Natl Acad Sci*. 1992:89(13):5951–5955.

Otsu Y, Couchman K, Lyons DG, Collot M, Agarwal A, Mallet JM, Pfrieger FW, Bergles DE, Charpak S. Calcium dynamics in astrocyte processes during neurovascular coupling. *Nat Neurosci*. 2015:18(2):210–218.

Ozus B, Liu HL, Chen L, Iyer MB, Fox PT, Gao JH. Rate dependence of human visual cortical response due to brief stimulation: an event-related fMRI study. *Magn Reson Imaging*. 2001:19(1):21–25.

Pastor MA, Artieda J, Arbizu J, Valencia M, Masdeu JC. Human cerebral activation during steady-state visual-evoked responses. *J Neurosci*. 2003:23(37):11621–11627.

Parkes LM, Rashid W, Chard DT, Tofts PS. Normal cerebral perfusion measurements using arterial spin labeling: reproducibility, stability, and age and gender effects. *Magn Reson Med*. 2004:51(4): 736–743.

Pasley BN, Inglis BA, Freeman RD. Analysis of oxygen metabolism implies a neural origin for the negative BOLD response in human visual cortex. *NeuroImage*. 2007:36(2):269–276.

Peng SL, Chen X, Li Y, Rodrigue KM, Park DC, Lu H. Age-related changes in cerebrovascular reactivity and their relationship to cognition: a four-year longitudinal study. *NeuroImage*. 2018:174: 257–262.

Perthen JE, Lansing AE, Liau J, Liu TT, Buxton RB. Caffeine-induced uncoupling of cerebral blood flow and oxygen metabolism: a calibrated BOLD fMRI study. *NeuroImage*. 2008:40(1):237–247.

Peters A, Sethares COligodendrocytes, their progenitors and other neuroglial cells in the aging primate cerebral cortex. *Cereb Cortex*. 2004:14(9):995–1007.

Petzold GC, Murthy VN. Role of astrocytes in neurovascular coupling. *Neuron*. 2011:71(5):782–797.

Podlutsky A, Ballabh P, Csiszar A. Oxidative stress and endothelial dysfunction in pulmonary arteries of aged rats. *Am J Phys Heart Circ Phys*. 2009.

Reuter-Lorenz PA. New visions of the aging mind and brain. *Trends Cogn Sci*. 2002:6(9):394–400.

Richards EM, Fiskum G, Rosenthal RE, Hopkins I, McKenna MC. Hyperoxic reperfusion after global ischemia decreases hippocampal energy metabolism. *Stroke*. 2007:38(5):1578–1584.

Rodríguez-Arellano JJ, Parpura V, Zorec R, Verkhratsky A. Astrocytes in physiological aging and Alzheimer's disease. *Neuroscience*. 2016:323:170–182.

Rombouts SA, Goekoop R, Stam CJ, Barkhof F, Scheltens P. Delayed rather than decreased BOLD response as a marker for early Alzheimer's disease. *NeuroImage*. 2005:26(4):1078–1085.

Ross MH, Yurgelun-Todd DA, Renshaw PF, Maas LC, Mendelson JH, Mello NK, Cohen BM, Levin JM. Age-related reduction in functional MRI response to photic stimulation. *Neurology*. 1997:48(1): 173–176.

Rypma B, Prabhakaran V, Desmond JE, Glover GH, Gabrieli JD. Load-dependent roles of frontal brain regions in the maintenance of working memory. *NeuroImage*. 1999:9(2):216–226.

Rypma B, D'Esposito M. Isolating the neural mechanisms of age-related changes in human working memory. *Nat Neurosci*. 2000:3(5):509–515.

Rypma B, D'Esposito M. Age-related changes in brain–behaviour relationships: evidence from event-related functional MRI studies. *Eur J Cogn Psychol*. 2001:13(1–2):235–256.

Rypma B, Prabhakaran V, Desmond JE, Gabrieli JD. Age differences in prefrontal cortical activity in working memory. *Psychol Aging*. 2001:16(3):371.

Rypma B, Berger JS, Prabhakaran V, Bly BM, Kimberg DY, Biswal BB, D'Esposito M. Neural correlates of cognitive efficiency. *NeuroImage*. 2006:33(3):969–979.

Salin K, Auer SK, Rey B, Selman C, Metcalfe NB. Variation in the link between oxygen consumption and ATP production, and its relevance for animal performance. *Proc R Soc B Biol Sci*. 2015:282(1812):20151028.

Schäfer K, Blankenburg F, Kupers R, Grüner JM, Law I, Lauritzen M, Larsson HB. Negative BOLD signal changes in ipsilateral primary somatosensory cortex are associated with perfusion decreases and behavioral evidence for functional inhibition. *NeuroImage*. 2012:59(4):3119–3127.

Smith ZM, Krizay E, Guo J, Shin DD, Scadeng M, Dubowitz DJ. Sustained high-altitude hypoxia increases cerebral oxygen metabolism. *J Appl Physiol*. 2013:114(1):11–18.

Singh M, Kim S, Kim TS. Correlation between BOLD-fMRI and EEG signal changes in response to visual stimulus frequency in humans. *Magn Reson Med*. 2003:49(1):108–114.

Sivakolundu DK, West KL, Zuppichini M, Turner MP, Abdelkarim D, Zhao Y, Spence JS, Lu H, Okuda DT, Rypma B. The neurovascular basis of processing speed differences in humans: a model-systems approach using multiple sclerosis. *NeuroImage*. 2020:215:116812.

Shetty PK, Galeffi F, Turner DA. Age-induced alterations in hippocampal function and metabolism. *Aging and disease*. 2011:2(3): 196.

Takano T, Tian GF, Peng W, Lou N, Libionka W, Han X, Nedergaard M. Astrocyte-mediated control of cerebral blood flow. *Nat Neurosci*. 2006:9(2):260–267.

Taneja K, Liu P, Xu C, Turner M, Zhao Y, Abdelkarim D, Thomas BP, Rypma B, Lu H. Quantitative cerebrovascular reactivity in normal aging: comparison between phase-contrast and arterial spin labeling MRI. *Front Neurol*. 2020:11:758.

Tarantini S, Tran CHT, Gordon GR, Ungvari Z, Csiszar A. Impaired neurovascular coupling in aging and Alzheimer's disease: contribution of astrocyte dysfunction and endothelial impairment to cognitive decline. *Exp Gerontol*. 2017:94:52–58.

Tarantini S, Balasubramanian P, Yabluchanskiy A, Ashpole NM, Logan S, Kiss T, Ungvari A, Nyúl-Tóth Á, Schwartzman ML, Benyo Z, et al. IGF1R signaling regulates astrocyte-mediated neurovascular coupling in mice: implications for brain aging. *Geroscience*. 2021:43(2):901–911.

Thesen T, Leontiev O, Song T, Dehghani N, Hagler DJ Jr, Huang M, Buxton R, Halgren E. Depression of cortical activity in humans by mild hypercapnia. *Hum Brain Mapp*. 2012:33(3):715–726.

Thomas BP, Liu P, Park DC, Van Osch MJ, Lu H. Cerebrovascular reactivity in the brain white matter: magnitude, temporal characteristics, and age effects. *J Cereb Blood Flow Metab*. 2014:34(2): 242–247.

Thomas CG, Menon RS. Amplitude response and stimulus presentation frequency response of human primary visual cortex using BOLD EPI at 4 T. *Magn Reson Med*. 1998:40(2):203–209.

Tian P, Teng IC, May LD, Kurz R, Lu K, Scadeng M, Hillman EMC, De Crespigny AJ, D'Arceuil HE, Mandeville JB, et al. Cortical depth-specific microvascular dilation underlies laminar differences in blood oxygenation level-dependent functional MRI signal. *Proc Natl Acad Sci*. 2010:107(34):15246–15251.

Trott DW, Seawright JW, Luttrell MJ, Woodman CR. NAD (P) H oxidase-derived reactive oxygen species contribute to age-related impairments of endothelium-dependent dilation in rat soleus feed arteries. *J Appl Physiol*. 2011:110(5):1171–1180.

Tsvetanov KA, Henson RN, Tyler LK, Davis SW, Shafto MA, Taylor JR, Williams N, Cam-CAN RJB. The effect of ageing on fMRI: correction for the confounding effects of vascular reactivity evaluated by joint fMRI and MEG in 335 adults. *Hum Brain Mapp*. 2015:36(6): 2248–2269.

Tsvetanov KA, Henson RN, Jones PS, Mutsaerts HJ, Fuhrmann D, Tyler LK, Rowe JB. The effects of age on resting-state BOLD signal variability is explained by cardiovascular and neurovascular factors. *bioRxiv*. 2019:836619.

Tsvetanov KA, Henson RN, Rowe JB. Separating vascular and neuronal effects of age on fMRI BOLD signals. *Philos Trans R Soc B*. 2021:376(1815):20190631.

Turner DA. Contrasting metabolic insufficiency in aging and dementia. *Aging and disease*. 2021:12(4):1081.

Turner MP, Hubbard NA, Sivakolundu DK, Himes LM, Hutchison JL, Hart J Jr, Spence JS, Frohman EM, Frohman TC, Okuda DT, et al. Preserved canonicality of the BOLD hemodynamic response reflects healthy cognition: insights into the healthy brain through the window of multiple sclerosis. *NeuroImage*. 2019:190:46–55.

Turner MP, Fischer H, Sivakolundu DK, Hubbard NA, Zhao Y, Rypma B, Bäckman L. Age-differential relationships among dopamine D1 binding potential, fusiform BOLD signal, and face-recognition performance. *NeuroImage*. 2019:206:116232.

Vafaee MS, Meyer E, Marrett S, Paus T, Evans AC, Gjedde A. Frequency-dependent changes in cerebral metabolic rate of oxygen during activation of human visual cortex. *J Cereb Blood Flow Metab*. 1999:19(3):272–277.

West KL, Zuppichini MD, Turner MP, Sivakolundu DK, Zhao Y, Abdelkarim D, Spence JS, Rypma B. BOLD hemodynamic response function changes significantly with healthy aging. *NeuroImage*. 2019:188:198–207.

West KL, Sivakolundu DK, Zuppichini MD, Turner MP, Spence JS, Lu H, Okuda DT, Rypma B. Altered task-induced cerebral blood flow and oxygen metabolism underlies motor impairment in multiple sclerosis. *J Cereb Blood Flow Metab*. 2021:41(1):182–193.

Wey HY, Wang DJ, Duong TQ. Baseline CBF, and BOLD, CBF, and CMRO 2 fMRI of visual and vibrotactile stimulations in baboons. *J Cereb Blood Flow Metab*. 2011:31(2):715–724.

Wolter KM. *Introduction to Variance Estimation (Vol. 53)*. New York (NY): Springer; 2007.

Xu F, Uh J, Brier MR, Hart J Jr, Yezhuvath US, Gu H, Yang Y, Lu H. The influence of carbon dioxide on brain activity and metabolism in conscious humans. *J Cereb Blood Flow Metab*. 2011:31(1):58–67.

Xu F, Liu P, Pascual JM, Xiao G, Lu H. Effect of hypoxia and hyperoxia on cerebral blood flow, blood oxygenation, and oxidative metabolism. *J Cereb Blood Flow Metab*. 2012:32(10):1909–1918.

Yabluchanskiy A, Nyúl-Tóth Á, Csiszar A, Gulej R, Saunders D, Towner R, Turner MP, Zhao Y, Abdelkarim D, Rypma B, et al. Age-related alterations in the cerebrovasculature affect neurovascular coupling and BOLD fMRI responses: Insights from animal models of aging. *Psychophysiology*. 2021:58(7):e13718.

Zappe AC, Uludağ K, Oeltermann A, Uğurbil K, Logothetis NK. The influence of moderate hypercapnia on neural activity in the anesthetized nonhuman primate. *Cereb Cortex*. 2008:18(11): 2666–2673.

Zhao Y, Liu P, Turner MP, Abdelkarim D, Lu H, Rypma B. The neural-vascular basis of age-related processing speed decline. *Psychophysiology*. 2021: in press.

Zhu XH, Kim SG, Andersen P, Ogawa S, Ugurbil K, Chen W. Dynamic study of BOLD, CBF, and $CMRO_2$ changes correlated to varied neuronal activity in primary visual cortex of humans. In: *Proceedings of the 6th Annual Meeting of the ISMRM*, Sydney. 1998. p. 10.

Zimmerman B, Rypma B, Gratton G, Fabiani M. Age-related changes in cerebrovascular health and their effects on neural function and cognition: A comprehensive review. *Psychophysiology*. 2021:58(7):e13796.